

Evaluation Microstructure and Hardness of the Fe-Cr-C Hardfacing Alloy with Cr/C=6 Ratio

H. Sabet*

Department of Materials Engineering, Karaj Branch, Islamic Azad University, Karaj, Iran.

Received 12 July 2021 - Accepted: 24 November 2021

Abstract

In this investigation, different amount of carbon and chromium content of Fe-Cr-C hardfacing alloys with the constant ratio of Cr/C=6 were used. These alloys were fabricated by GTAW on AISI 1010 mild steel substrates to achieve hypo/eutectic/hyper compositions. OES, XRF, OM, SEM, XRD techniques and HV method were used for determining chemical composition, hardness and studying the microstructure of hardface alloys. The metallographic examination results indicated that all hardface samples had three metallurgical zones with different thickness, microhardness, chemical composition and solidification modes. The microstructures of all hardface samples in thicker Zone consists of austenite and chromium-iron carbides $(Cr,Fe)_7C_3$. Moreover with increasing of carbon and chromium content of thicker zone in hardface samples, the volume fraction of $(Cr,Fe)_7C_3$ increased and resulted in the decreasing of austenite volume fraction and increasing hardness of the top surface. A multiple regression model was used to determine the relation between microstructure, chemical composition and hardness.

Keywords: Alloys, Cr/C=6, Surface Modification, Microstructure, SEM.

1. Introduction

Wear is one of the most frequently encountered failure modes for mechanical components [1]. Hardfacing is a commonly employed method to improve wear resistance properties of these equipments [2]. A wide variety of hardfacing alloys are commercially available for use and controlling of wear [3, 4]. Three types of these alloys which commonly used for hardfacing of steels are [4-6]: Fe-Cr-C, Fe-C-X (X= carbide former elements) and Fe-Ni-Co. The Fe-Cr-C is the most popular type of hardfacing alloy because its cost is relatively lower than those of the others [5, 6]. These alloys are used in severe abrasive wear conditions such as the mining and cement industries [6, 7]. The good abrasive wear resistance in these alloys is due to the formation of high volume fraction of carbides in a tougher matrix [7]. The types of carbides such as M_7C , M_7C_3 and $M_{23}C_6$ in Fe-Cr-C alloys are dependent upon the Cr/C ratio, therefore this ratio determines the applicable alloys in different wear conditions [8, 9]. It is noted that [9] an excellent abrasive wear resistance can be obtained in the ratio Cr/C=5-8, in which the $(Cr,Fe)_7C_3$ carbides with Cr-rich austenite appears in the microstructure. Hypoeutectic, eutectic and hypereutectic compositions have been seen in these types of hardfacing layers [9, 10].

Most investigations focus on the relation between wear properties and microstructure or chemical composition in Fe-Cr-C hardfacing alloys. Dasgupta et.al [11] suggested that the wear resistance of these alloys was only improved with a Cr content of more than 3%. Jha et.al [12] reported that the high chromium and low carbon (Cr/C=13) content of Fe-Cr-C hardfacing alloy resulted in better wear resistance than low chromium and high carbon content (Cr/C=1.1). Dwiredi [13] reported that the hardfacing layer with a Cr/C ratio of 7 shows a better wear resistance than that with a ratio of 10.

Liu et.al [14] studied the microstructure of Fe-Cr-C alloy and reported that better microstructure for excellent wear resistance was obtained in the case of coarse primary $(Cr,Fe)_7C_3$ carbides that were uniformly distributed in the fine, strong and ductile $(Cr,Fe)_7C_3/\gamma Fe$ eutectics matrix. Similar results were also reported by others such as Choteborsky [15], Cheng et.al [16], Buchanan et.al [17] and Buchely et.al [18]. Recently, Chang et.al [19] focused on the effect of the carbon content on microstructure and hardness of Fe-Cr-C hardfacing alloys at constant chromium (40%). Their studies showed that by increasing of carbon from 1.35% (Cr/C=32) to 4.05% (Cr/C=10), different microstructures such as hypoeutectic, eutectic and hypereutectic with different hardness were appeared. In addition, the maximum hardness of hardface layers obtained in Fe-40%Cr-4.05%C attributed to massive hard $(Cr,Fe)_7C_3$ carbides. In other research, Chang et.al [20] reported that in hypereutectic Fe-Cr-C hardface alloys (in constant chromium), with increasing of carbon content from

*Corresponding author

Email address: h-sabet@kiaau.ac.ir

3.73% (Cr/C=7) to 4.85% (Cr/C=5.5), the amounts of primary (Cr,Fe)₇C₃ carbides were increased and its sizes were reduced. Moreover maximum hardness was obtained when (Cr,Fe)₇C₃ carbides volume fraction reached 86% with minimum size 13.53 μm, although this condition achieved at the ratio of Cr/C=5.5.

Although many researchers have been studying the Fe-Cr-C microstructure and its relationship with hardness, but in using constant Cr/C ratios, there seems to be no systematic detail available and not yet investigated. Therefore, this study establishes the relationship between chemical composition (Cr% and C%) at a constant ratio of Cr/C=6 with the microstructure and hardness of Fe-Cr-C hardfacing alloy.

2. Materials and Methods

AISI 1010 mild steel specimens with dimensions of 200×120×10 mm were used as substrate.

The chemical composition of the steel that is determined by OES is given in Table. 1. The surfaces of samples were prepared in 4 steps:

1. Surface grinding (1mm) to eliminate any contaminants layers
2. Thorough cleaning by water
3. Drying by hot air, and
4. Rinsing by acetone.

As coating materials, six powder mixtures with different ferrochromium to crystalline graphite weights, but in constant Cr/C=6 ratio were used. The chemical composition ferrochromium and crystalline graphite that determined by XRF are shown in Table. 1.

The powders were mixed in a laboratory ball mill with 200Cm³ internal volume area at argon gas atmosphere for 1 hour, then the mixture of powders was sieved and weighted, and the average particles sizes were determined by distribution curve. The average size of powders after mixing was 30^{μm}. Then the powders were mixed with 20 wt. % sodium silicate binder in a laboratory mixer for 5 minutes. These mixed powders were preplaced in 1×70×200 mm on the surface of steel substrates with different area density (Table. 2.), and dried in an electrical furnace at 120 °C for 1 hour [21]. Table. 3. shows the surface GTAW treatment parameters.

Table. 1. Chemical compositions (wt.%) of the specimen (AISI 1010) and powders for surface alloying.

Material	C	Si	Mn	P	S	Cr	Fe
AISI 1010	0.081	0.18	0.33	0.01	0.01	-	Bal.
Ferrochromium	0.054	0.24	0.1	0.01	0.01	69	Bal.
Crystalline Graphite	99.79	0.03	0.03	0.06	0.09	-	-

Table. 2. Area Density of preplaced powders.

No of samples	1	2	3	4	5	6
Area Density (gr/cm ²)	0.85	1	1.15	1.3	1.4 5	1.6

Table. 3. Surface GTAW treatment parameters.

Process	Automatic GTAW	Welding speed (Cm/min)	10	Number of layers tracks	8
Polarity	DCEN	Electrode type	EWTh-2	Overlap of layers tracks	20%
Current (A)	100	Electrode tip (angel)	60	Number pass of each track	2
Voltage (V)	14	Gas shield	Pure argon	Heat in put (Kj/mm) of each track	0.5
Arc length (mm)	3	Gas flow (Lit/min)	8		

To produce a series of multiple hardfacing passes, track Surface alloying technique was carried out by using GTAW heat source, as shown in Fig. 1.

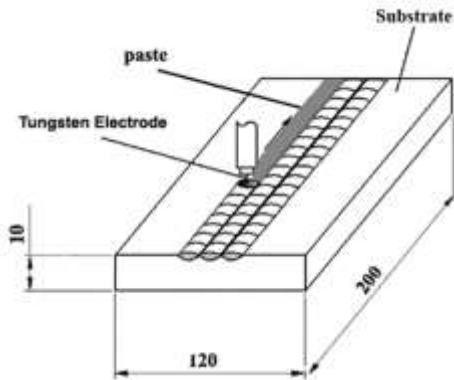


Fig. 1. Schematic of surface alloying by GTAW.

Chemical analysis was done by optical emission spectrum (OES) equipped with the charge coupled device (CCD) technology at the 1 mm depth of the surface. The metallographic samples were prepared by using SiC grinder paper, 1 μm diamond paste polisher, and 2% nital solution etchant. In addition, the special etchant [22] was also used to determine the volume fraction of phases by using an image analysis. The microstructure characterization of each sample was observed by a Scanning Electron Microscope (VEGA/TESCAN) using BSE, EDS and WDS analysis. XRD samples were cut to 10X10X3 mm dimensions and were prepared by mechanical and electro polished [23]. XRD was carried out by a diffractometer (STAPI MP) equipped with x pert high score, using copper k-alpha ($\lambda=1.54\text{\AA}$) radiation and a nickel filter. The θ angle was 10-90 $^\circ$ with a step size of 0.04 and a time step of 8 second per step. The hardness of the top surface was established by using Vickers macrohardness method (KOOA universal UA1) with 30000 gr load.

The microhardness was performed by the Vickers hardness tester (Struers -Duramin) with 100 gr load on the cross-section of the samples. Moreover, for determining the relationship between chemical composition of hardface alloys (Cr%, C %) and the amount of phases involved in microstructure, a multiple regression method was used by regression calculator (Demo -9.8 -2007) software.

3. Results and Discussion

3.1. Chemical Composition and Microstructure

Fig. 2. shows the microstructure characteristics of the bonding interface between the hardface coating and the substrate of sample 6 in transverse cross section. It can be seen that high quality metallurgical bonding (without cracks and porosity) occurs between hardface coating and steel substrate. Moreover, three different metallurgical zones can be seen from bonding interface to top surface, these zones were observed in all hardface samples. Table. 4. gives specifications of the three metallurgical zones in all hardface samples.

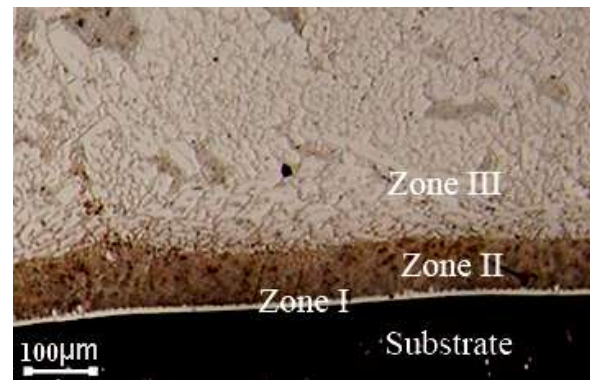


Fig. 2. OM micrograph transverse cross section of sample No 6.

Table. 4. Metallurgical zones specifications* of samples

No of Sample	1			2			3		
	Thickness (μm)	Chemical composition (wt. %)		Thickness (μm)	Chemical composition (wt. %)		Thickness (μm)	Chemical composition (wt. %)	
		Cr	Fe		Cr	Fe		Cr	Fe
Zone I	7.8	1.97	98.03	8.9	2.09	97.91	9.6	2.16	97.84
Zone II	88	3.93	96.07	89	5.17	94.83	93	6.39	93.61
Zone III	2510	8.82	91.18	2580	12.03	87.97	2570	15.11	84.89
No of Sample	4			5			6		
	Thickness (μm)	Chemical composition (wt. %)		Thickness (μm)	Chemical composition (wt. %)		Thickness (μm)	Chemical composition (wt. %)	
		Cr	Fe		Cr	Fe		Cr	Fe
Zone I	8.6	2.19	97.81	10	2.23	97.77	9.3	2.26	97.74
Zone II	98	8.16	91.84	93	10.01	89.09	96	11.91	88.09
Zone III	2550	18.21	81.79	2490	20.88	79.12	2520	23.92	76.18

* The chemical compositions of different zones are determined by the EDS method.

Table. 4. shows that the three metallurgical zones had different thickness and chemical composition. Zone I in all hardface samples is observed at the closed of substrate with maximum $10\ \mu\text{m}$ thickness. Furthermore, it can be seen that in all hardface samples, the iron and chromium concentrations of this zone are almost equal.

The reason of this maybe that Zone I has high iron and low chromium content with 80-90 % dilution with substrate. In addition this zone had high ratio of G/R ; where G is; temperature gradient and R is ; Growth rate [19, 24,25]. Solidification of this zone started with epitaxial growth and planer front solidification with high solidification rate [24,25],as the austenite with martensite microstructure observed in this zone in all hardface samples. Fig. 3. illustrates the SEM micrograph of the Zone I in sample 1.

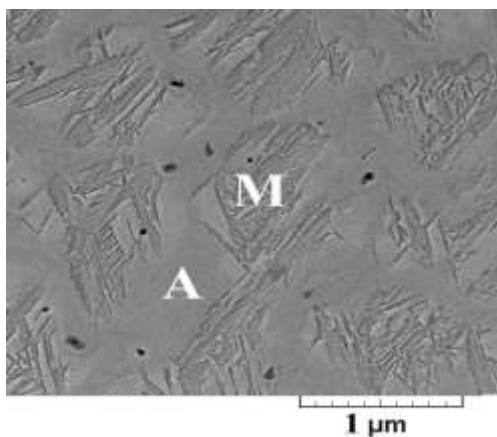


Fig. 3. SEM micrograph of Zone I in sample 1.

Zone II with maximum $100\ \mu\text{m}$ thickness is observed over Zone I. In all hardface samples this Zone has 50-60% dilution with lower G/R ratio and solidification rate than those of Zone I [5, 19,24, 25]. Table. 4. shows that in all samples this zone has higher chromium concentration than the Zone I, Therefore solidification of this Zone is dependent on the chemical composition [19, 24, 25]. Metallographic results of these zones in hardface samples shows different microstructures, owing to the rapid increase of solidification rate at the interface, destabilized the planer front lead [24] to the formation of Fe-Cr-C alloys.

In samples of No 1 to 4, this zone consisted of a complex structure of eutectic $\gamma+(\text{Cr,Fe})_7\text{C}_3$ and globular primary austenite. In sample No 5, a complex of eutectic $\gamma+(\text{Cr,Fe})_7\text{C}_3$ and very fine globular austenite, and in sample No. 6, eutectic $\gamma+(\text{Cr,Fe})_7\text{C}_3$ structure had wrought. Fig. 4. illustrates the SEM micrograph bonding along the transverse cross sections of Zones I and II in samples No. 1, No. 5 and No. 6.

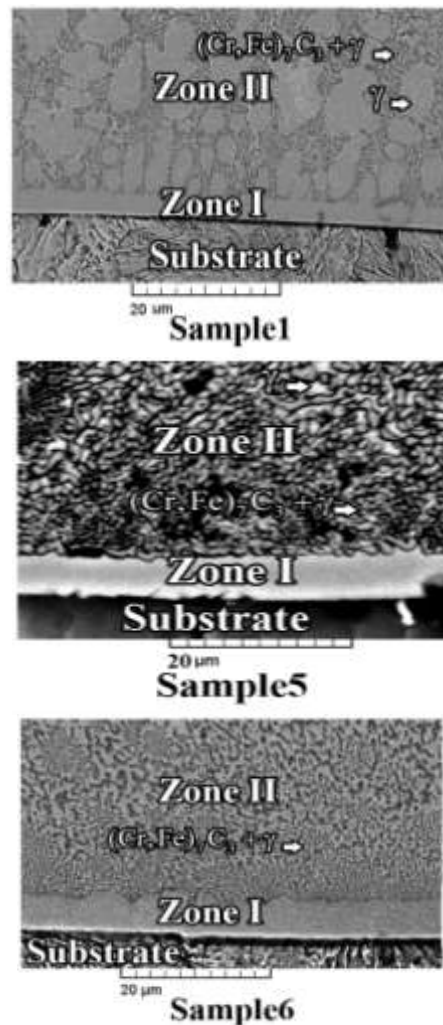


Fig. 4. SEM micrographs of transverse cross sections of Zones I and II in different samples.

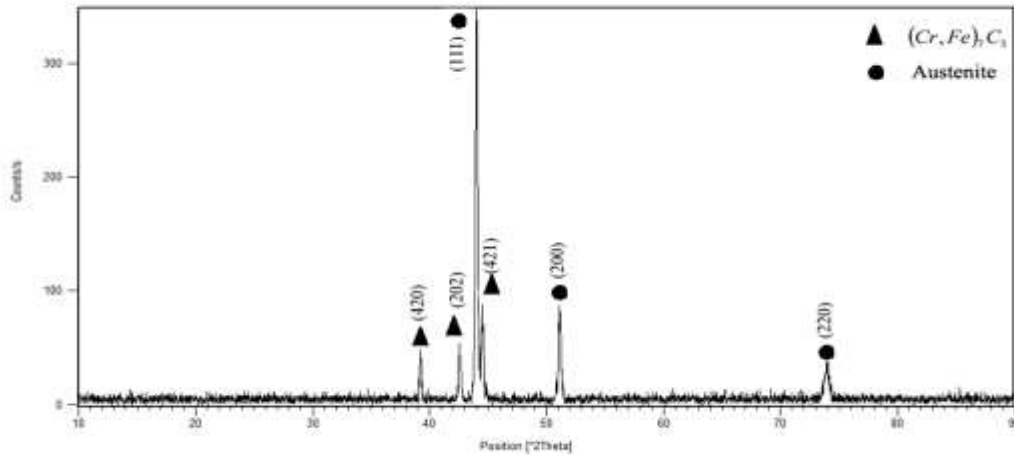
Zone III with maximum thickness is observed over Zone II up to the top surface. The chemical compositions of these zones (Table. 4.) show that these zones have high chromium and low iron concentrations in comparison with the other zones. In all hardface samples this zone is an essential zone because it is thicker and has minimum dilution (2-10%) with the lowest G/R ratio and solidification rate [5,19, 25] in comparing with other zones. Owing to this, hypo, eutectic and hypereutectic Fe-Cr-C compositions and microstructures can be observed in these zones.

Table. 5. provides chemical composition (wt. %) of the Zone III in hardface samples. From Table. 5. it is denoted that all hardface samples have the same $\text{Cr}/\text{C} \cong 6$, but different carbon and chromium contents. According to the Fe-C-Cr phase diagram [26, 27], samples of No. 1 to No. 4 have hypoeutectic compositions, while samples No. 5 and No. 6 have eutectic and hypereutectic composition respectively.

Table 5. Chemical composition* (wt. %) of Zone III in hardface samples.

No of Sample	Chemical composition (wt. %)							Cr/C	Type of solidification
	C	Si	Mn	P	S	Cr	Fe		
1	1.43	0.11	0.13	0.002	0.002	8.93	Bal	6.2	hypoeutectic
2	1.94	0.13	0.14	0.002	0.003	12.22	Bal	6.3	hypoeutectic
3	2.45	0.12	0.14	0.002	0.002	15.32	Bal	6.2	hypoeutectic
4	2.97	0.11	0.13	0.002	0.003	18.62	Bal	6.2	hypoeutectic
5	3.52	0.13	0.12	0.002	0.003	21.32	Bal	6.1	eutectic
6	4.02	0.12	0.13	0.002	0.002	24.22	Bal	6.0	hypereutectic

*Determined by OES method in 1 mm under the top surface

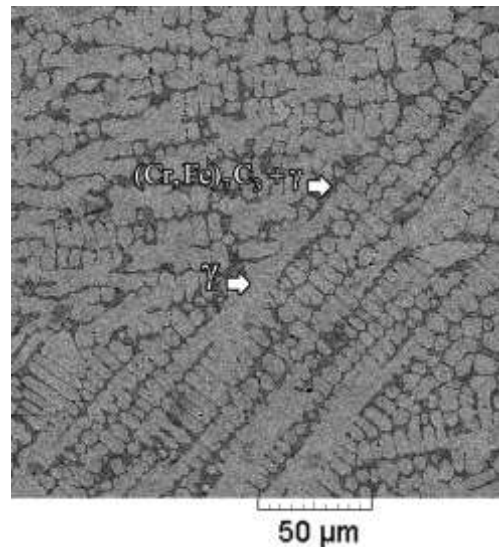
**Fig. 5. XRD pattern of the Zone III of sample No 1 with hypoeutectic composition.**

The XRD pattern of the zone III of sample No 1 with hypoeutectic composition with the 1.43% C, 8.93% Cr, and Cr/C=6.2 is shown in Fig. 5.

In this pattern austenite and $(Cr,Fe)_7C_3$ peaks can clearly be seen. Solidification in hypoeutectic composition of Fe-Cr-C alloys is started with nucleation and growth of austenite in the temperature range of 1400-1450 °C [26, 27].

In Fe-Cr-C ternary system, by increasing [27] of chromium content the solubility of carbon in austenite is decreased. When the austenite is grown in the melt, the carbon content of the remained liquid phase is increased gradually to approach to the eutectic composition, so the eutectic reaction of $L \rightarrow \gamma + (Cr,Fe)_7C_3$ occurs when the temperature reaches 1240 °C. Finally, at room temperature there are primary austenite and $\gamma + (Cr,Fe)_7C_3$ eutectic in the microstructure [5, 27, 28]. Fig. 6. shows the microstructure of the Zone III of sample No 1; it can be seen that hypoeutectic structure is obtained with primary austenite dendrites and $\gamma + (Cr,Fe)_7C_3$ eutectic structure. The stability of austenite at room temperature in this sample is due to the relationship between martensite start temperature (M_s) and the chemical composition (C%, Cr %) of the austenite, the relation between M_s Temperature (°C) and the chromium and carbon contents of the austenite in Fe-Cr-C alloys is [29]:

$$M_s = 383.11 - 207.42(C\%) - 20.65(Cr\%) \quad \text{Eq. (1).}$$

**Fig. 6. SEM micrograph of the Zone III of sample No1 with hypoeutectic composition .**

The Chemical composition of the austenite in Zone III of sample No. 1 determined by WDS method is given in Table. 6. If the average carbon and chromium content of austenite is replaced in Eq. (1), the M_s for transformation of austenite to martensite in sample No. 1 with hypoeutectic composition can be calculated as:

$$M_s = 383.11 - 207.42(1.19) - 20.65(7.23) = -13 \text{ } ^\circ\text{C}$$

Since the M_s is dropped to below room temperature, no martensite is appeared in the microstructure of this sample.

The XRD pattern of the Zone III of sample No. 6 with hypereutectic composition with the 4.02% C, 24.22% Cr, and Cr/C = 6.0 is shown in Fig. 7. The $(Cr,Fe)_7C_3$ Carbides with austenite can be seen in this pattern In hypereutectic composition of Fe-Cr-C alloys, solidification is started with nucleation and growth of primary carbides $(Cr,Fe)_7C_3$ at 1375 °C [26-28]. During growth of primary carbides in melt, the carbon content is reduced and finally when the remained melt approaches an eutectic temperature, its composition reaches to non

equilibrium eutectic composition and the reaction of $L \rightarrow \gamma + (Cr,Fe)_7C_3$ occur at 1280 °C [27, 28,30]. At room temperature the structure consists of primary carbides $(Cr,Fe)_7C_3$ and austenite+ $(Cr,Fe)_7C_3$ eutectic [25, 27,30].

Fig. 8. shows the microstructure of the zone III of sample No. 6 with hypereutectic composition. This figure includes the hexagonal - shape primary $(Cr,Fe)_7C_3$ and a typical eutectic austenite + $(Cr,Fe)_7C_3$ structure.

Table. 7. shows the microstructure characteristics of the Zone III of different hardface samples.

Table. 6. Chemical composition of austenite in Zone III of sample No 1 with hypoeutectic composition.

No of exam	Element (wt %)				
	C	Cr	Si	Mn	Fe
1	1.260	7.680	0.120	0.240	90.700
2	1.140	7.060	0.130	0.290	91.380
3	1.170	6.950	0.080	0.280	91.520
Average	1.190	7.230	0.110	0.270	91.200

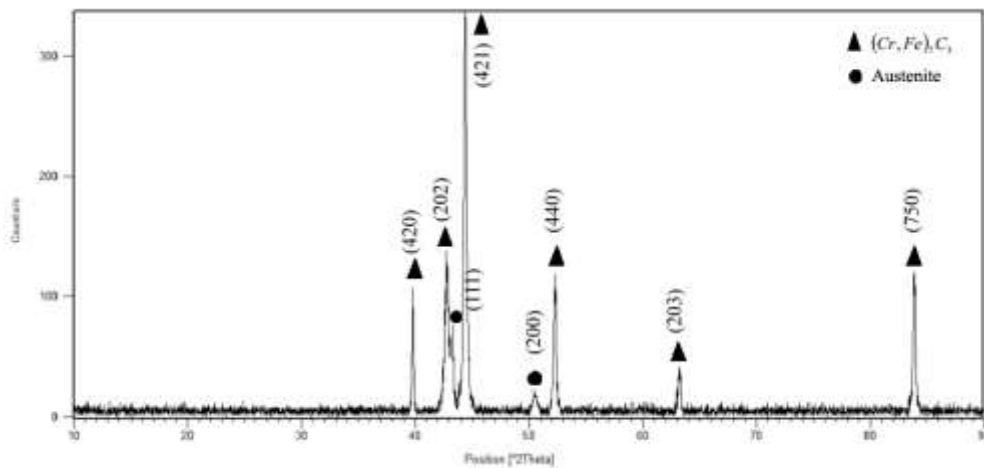


Fig. 7. XRD pattern of the Zone III of sample No 6 with hypereutectic composition.

Table. 7. The microstructure characteristics* of the Zone III of different samples .

No of Sample	Chemical Composition (wt. %)		Solidification Mode	Microstructure (%vol)							
	C	Cr		Primary austenite	Eutectic austenite	Total austenite	Primary carbide	Eutectic carbide	Total carbide	Eutectic phase	EC / EA **
1	1.42	8.93	hypoeutectic	63	10	73	-	27	27	37	2.7
2	1.94	12.22	hypoeutectic	45	14	59	-	41	41	54	2.9
3	2.46	15.32	hypoeutectic	30	17	47	-	53	53	70	3.1
4	2.97	18.62	hypoeutectic	16	20	36	-	64	64	84	3.2
5	3.52	21.32	eutectic	-	23	23	-	77	76	100	3.3
6	4.02	24.22	hypereutectic	-	15	15	45	40	85	55	2.6

* Measured by image analysis

$$\frac{EC}{EA} = \frac{\text{Eutectic Carbide}}{\text{Eutectic Austenite}}$$

**

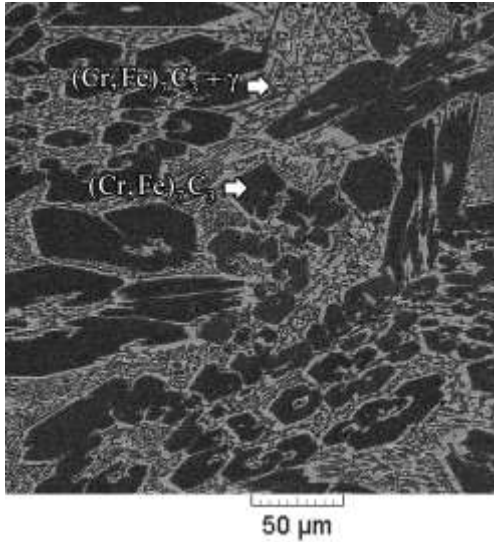


Fig. 8. SEM micrograph of the Zone III of Sample No 6 with hypereutectic composition.

Fig. 9. And Fig. 10. shows the relation between volume fraction of primary austenite and eutectic phases (carbide and austenite) in microstructure with carbon and chromium content of different hardface samples. According to the Fe-Cr-C phase diagram [26], by increasing of carbon and chromium content of the hypoeutectic compositions, decreasing in the solidification range occurs. As volume fraction of primary austenite decreases, volume fraction of the melt (eutectic composition) increases. Therefore by increasing the carbon and chromium content of hypoeutectic composition (sample No. 1-4) the amount of primary austenite decreases and eutectic phase increases, while the amount of $(Cr,Fe)_7C_3$ eutectic carbides and eutectic austenite are increasing. In the eutectic composition (sample No 5) austenite and carbide that appeared in the microstructure are eutectic phases.

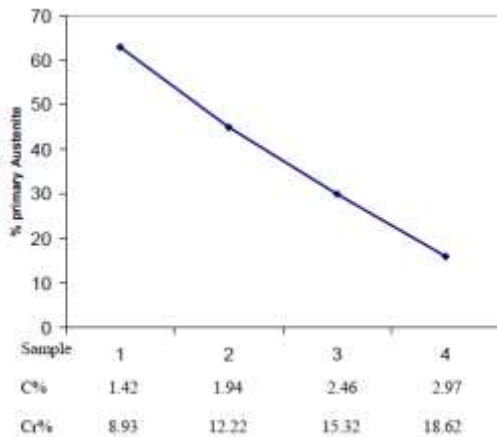


Fig. 9. Relation between volume fraction of primary austenite microstructure with carbon and chromium content of different hardface samples.

In hypereutectic composition (sample No. 6) high amounts of primary carbides are formed and the

remained melts were transformed to eutectic microstructure [26, 27, 30,31].

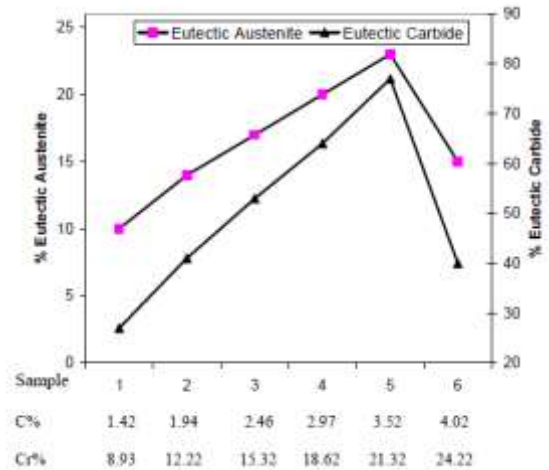


Fig. 10. Relation between volume fraction of eutectic phases microstructure with carbon and chromium content of different hardface samples.

In addition results of Table. 7. and Fig. 10., shows that the ratio of eutectic carbides to eutectic austenite, was increased to eutectic composition and then was decreased in hypereutectic composition. In Fe-Cr-C phase diagram [26-30] by increasing of carbon and chromium concentrations in chemical composition, eutectic point and eutectic composition fell to less concentrations.

Fig. 11. shows the relation between total austenite and carbides in microstructure with carbon and chromium content of different hardface samples, it can be recognized that when total carbides were increased, the amount of austenite were decreased. In fact, increasing the carbon and chromium content in the melt causes an increase in the activity of these elements and the tendency of carbides production will be increased, so the amount of produced carbides will be increased [29-33].

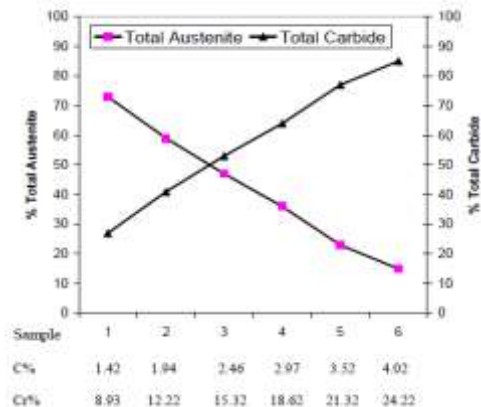


Fig. 11. Relation between total austenite and carbides in microstructure with carbon and chromium content of different hardface samples

Results analysis of microstructural characteristics of the Zone III of different samples, denotes that can be written the following formula to determine the relationship between the chemical composition and the amount of total carbides and austenite in Zone III of Fe-Cr-C hardface coating in this research, hence by using the multiple regression method determine:

$$\text{Total Carbides vol\%} = 17.5(\text{C\%}) + 1.2(\text{Cr\%}) - 9.9$$

With $R=0.97$ Eq. (2).

$$\text{Total Austenite vol\%} = 100 - \text{vol\% Total Carbide}$$

With $R=0.97$ Eq. (3).

$$\text{Total Austenite vol\%} = [(C\%) + (Cr\%)] \cdot 0.97$$

With $R=0.98$ Eq. (4).

Where: C%=Weight percent of carbon, and Cr%=Weight percent of chromium contents of the Zone III of hardface alloys.

3.2. Hardness

Fig. 12. shows the microhardness of different zones of the selective samples with various chemical compositions (hypo/eutectic/hyper). It can be seen that the microhardness of Zone I in different samples have the same values. Owing to the chemical composition (Fe and Cr content) and microstructure of this zone are almost the same (Table. 5.), whereas in Zone II and Zone III, due to the difference in the chemical composition and microstructure of these zones, different microhardnesses were achieved. Comparison of the microhardness amounts of Zones II and III of the various samples show that, by increasing of carbon and chromium content of the chemical composition, the microstructure characteristics is changed and the microhardness of Zone II and Zone III is increased.

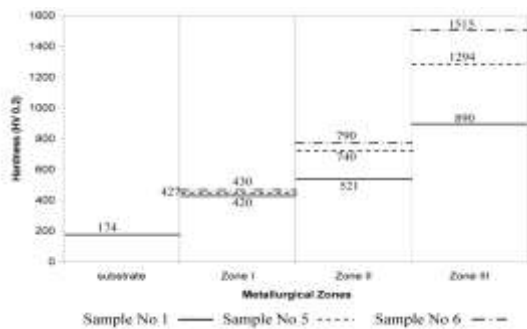


Fig. 12. Microhardness of different zones of sample 1, 5 and 6.

The maximum microhardness amounts of Zones II and Zones III are associated to sample No 6 with hypereutectic composition, because in zone II hasn't primary austenite, and in zone III has

maximum total $(\text{Cr,Fe})_7\text{C}_3$ carbides with minimum total austenite in microstructure. Owing to different volume fraction of austenite and carbides the microhardness amount of the Zones II and III of eutectic composition (sample No. 5) more than hypoeutectic composition (Sample No. 1). From Fig. 4. denote that volume fraction of primary austenite in zone II of eutectic composition (No. 5) less than hypoeutectic composition (No. 1), and in zone III (Table. 7. and Fig. 11.) has the more total carbides than that hypoeutectic composition.

Fig. 13. shows the macrohardness of the top surface of all hardface samples in zone III. The outcome of this Figure exhibits that the hardness of hardface coating increases by increasing the volume fraction of total carbides $[(\text{Cr,Fe})_7\text{C}_3]$, so that the highest amount of hardness was gained in sample No. 6, in which there is 85% total carbide and 15% total austenite.

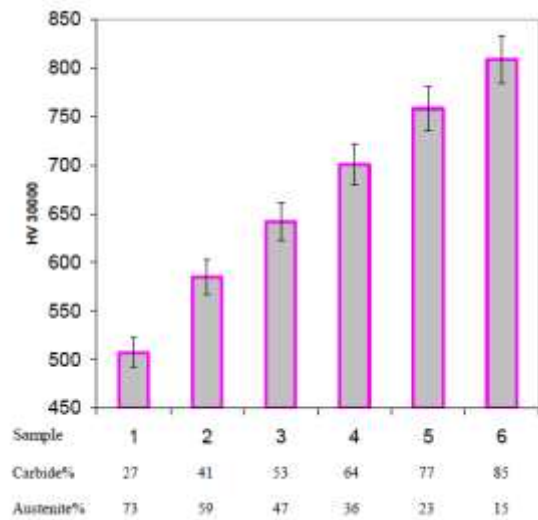


Fig. 13. Surface layers hardness of top of the Zone III in different hardface samples.

Eq. (4). shows the relationship between hardness and volume fraction of carbide and austenite, using multiple regression method:

$$1.9(\text{Total Austenite}) + 6.7(\text{Total Carbide}) + 195 = \text{HV}$$

With $R=0.96$ Eq. (5).

4. Conclusion

1. All hardface samples had 3 metallurgical zones, with different thickness, microhardness, chemical composition and solidification modes. Essential zones were observed near the surface.
2. In all samples, Zone I had epitaxial growth with planer front solidification, Zone II, had eutectic Fe-Cr-C structure, Zone III was an essential layer of hardface coating, and solidify proportionate of the chemical composition (hypo/eutectic/hyper).
3. In all samples the microstructure of thicker Zone (III) is composed of austenite and chromium

carbides as $(Cr,Fe)_7C_3$, but various chemical compositions make different type of solidification and exist hypo/hyper/and eutectic microstructure.

4. By increasing the carbon and chromium content of Zone III in hardface samples, the volume fraction of carbides $[(Cr,Fe)_7C_3]$ increase and austenite in microstructure decreases.

5. By increasing the carbon and chromium content of Zone III in the hypoeutectic compositions, volume fraction of primary austenite decreases and volume fraction of the eutectic austenite and carbides increases, in hypereutectic composition, volume fraction of the eutectic carbide and austenite are less than those of eutectic composition.

6. In Fe-Cr-C hardface alloys the relationship between chemical compositions (Cr%, C%) and microstructure(Carbides%, Austenite%) in Zone III can be estimated as:

$$\text{Total Carbides vol\%} = 17.5(C\%)+1.2(Cr\%)-9.9$$

$$\text{Total Austenite vol\%} = 100 - \text{vol\% Total Carbide}$$

$$\text{Eutectic Austenite vol\%} = [(C\%)+(Cr\%)]0.97$$

7. By increasing the carbon and chromium content of the chemical composition, the microhardness of Zone II and Zone III increases. Maximum microhardness value of Zones II and III is related to the hypereutectic composition.

8. In Fe-Cr-C, hardness of top surface layers (Zone III) dependence with microstructure (Carbides%, Austenite %) and correlated as following formula:

$$1.9(\text{Total Austenite})+6.7(\text{Total Carbide})+195=HV$$

References

- [1] Y. F. Liu, Z. Y. Xia, J. M. Han, G. L. Zhang and S. Z. Yang, *Surf. Coat. Technol.*, 201, (2006) 863.
- [2] J. J. Coronado, H. F. Caicedo and A. L. Gomez, *Tribol. Int.*, 42, (2009), 745.
- [3] M. Erolgu, *Surf. Coat. Tech.*, 203, (2009), 2229.
- [4] K. Y. Lee, S. H. Lee, Y. Kim, H. S. Hong, Y. M. Oh and S. J. Kim, *Wear*, 225, (2003), 481.
- [5] S. Buytoz, M. M. Yildirim and H. Eren, *Mater. Lett.*, 59, (2005), 607.
- [6] M. Kirchgabner, E. Badisch and F. Franek, *Wear*, 265, (2008), 772.
- [7] J. Liu, L. Wang and J. Huang, *J. Univ. Sci. Technol. Beijing*, 13, 6, (2006), 538.
- [8] S. Atamert and H. K. D. H. Bhadeshia, *Mater. Sci. Eng. A*, 130, (1990), 101.
- [9] E. Zumelzu, I. Goyos, C. Cabezas, O. Poitz and A. Parada, *Mater. Process. Technol.*, 128, (2002), 250.
- [10] C. M. Chang, Y. C. Chen and W. WU, *Tribol. Int.*, 43, (2010), 929.
- [11] R. Dasgupta, R. Thakur, M. S. Yadav and A. K. Jha, *Wear*, 236, (1999), 368.
- [12] A. K. Jha, B. K. Prasad, R. Dasgupta and O. P. Modi, *J. Mater. Eng. Perform.*, 8, 2, (1999), 190.
- [13] D. K. Dwiredi, *Mater. Sci. Technol.*, 20, (2004), 1326.
- [14] Y. F. Liu, J. M. Han, R. H. Li, W. J. Li, X. Y. Xu, J. H. Wang and S. Z. Yang, *Appl. Surf. Sci.*, 252, (2006), 7539.
- [15] R. Choteborsky, P. Hrabe, M. Muller, J. Sarkoca and M. Jirka, *Res. Agr. Eng.*, 4, 54, (2008), 192.
- [16] J. B. Cheng, B. S. XU, X. B. Liang and Y. W. Wu, *Mater. Sci. Eng. A*, 492, (2008), 407.
- [17] V. E. Buchanan, P. H. Shipwey, D. G. MC Cartney, *Wear*, 263, (2007), 99.
- [18] M. F. Buchely, J. C. Gutierrez, L. M. Leon and A. Toro, *Wear*, 259, (2005), 52.
- [19] C. M. Chang, C. M. Lin, C. C. Hsieh, J. H. Chen and W. Wu, *J. Alloys Compd.*, 487, (2009), 83.
- [20] C. M. Chang, C. M. Lin, C. C. Hsieh, J. H. Chen, C. M. Fan and W. Wu, *Mater. Chem. Phys.*, 117, (2009), 257.
- [21] M. Eroglu and N. Ozdemir, *Surf. Coat. Technol.*, 154, (2002), 209.
- [22] W. K. Collins and J. C. Watson, *Mater. Charact.*, 24, 4, (1990), 379.
- [23] S. D. Carpenter and D. Carpenter, *Mater. Lett.*, 57, (2003), 4456.
- [24] C. M. Lin, C. M. Chang, J. H. Chen, C. C. Hsieh and W. Wu, *Metall. Mater. Trans. A*, 40A, May, (2009), 1031.
- [25] S. Buytoz, *Mater. Lett.*, 60, (2006), 605.
- [26] D. Li, L. Liu, Y. Zhang, C. Ye, X. Ren, Y. Yang and Q. Yang, *Mater. Des.*, 30, (2009), 340.
- [27] A. Bondar, V. Ivanchento, A. Kozbv and J. C. Todenac, *Group IV – Springer-Verlag Berlin Heidelberg*, Vol. 11, (2008) 1.
- [28] O. N. Dogan, J. A. Hawk and G. Laird II, *Metall. Mater. Trans. A*, 28A, June (1997), 1315.
- [29] K. Yamamoto, M. M. Liliac and K. Ogi, *Int. J. Cast. Met. Res.*, 16, 4, (2003), 435.
- [30] C. M. Chang, L. H. Chen, C. M. Lin, J. H. Chen, C. M. Fan and W. Wu, *Surf. Coat. Technol.*, 205, (2010), 245.
- [31] R. J. Chung, X. Tang, D. Y. Li, B. Hinckley and K. Dolman, *Wear*, 301, (2013), 695.
- [32] H. Sabet, SH. Kheirandish, SH. Mirdamadi, M. Goodarzi, *Tirb.lett*, Vol. 44, (2011), 237
- [33] J. H. Chen, C. C. Hsieh, P. S. Hua, C. M. Chang, C. M. Lin, P. Ti-Y. Wu and W. Wu, *Met. Mater. Int.*, Vol. 19, No. 1 (2013), 93.